

# High-resolution petrographic evidence confirming detrital and biogenic magnetites as remanence carriers for Zongpu carbonates in the Gamba area, South Tibet

1 Qian Zhao<sup>1</sup>, Baochun Huang<sup>1\*</sup>, Zhiyu Yi<sup>2</sup>, Pengfei Xue<sup>1</sup>

2 <sup>1</sup> Key Laboratory of Orogenic Belt and Crustal Evolution, Ministry of Education, School of Earth  
3 and Space Sciences, Peking University, Beijing, China

4 <sup>2</sup> Planetary Environmental and Astrobiological Research Laboratory (PEARL), School of  
5 Atmospheric Sciences, Sun Yat-sen University, Zhuhai, China

6 \* **Correspondence:**

7 Baochun Huang  
8 bchuang@pku.edu.cn

9 **Keywords: Magnetic extraction, Carbonates, Paleomagnetism, Tethyan Himalaya, Paleocene**

## 10 **Abstract**

11 Paleocene carbonates from the Gamba area of South Tibet provide the largest paleomagnetic  
12 dataset for constraining the paleogeography of the India-Asia collision in the early stage. The  
13 characteristic remanences (ChRMs) obtained from this unit were, however, argued for a chemical  
14 remagnetization via orogenic fluids. This study carries out a high-resolution petrographic study on  
15 the Paleocene carbonates from Gamba aiming to test the nature of the ChRMs. Electron microscopic  
16 observation on magnetic extracts identified a large amount of detrital magnetite that are multi- to  
17 single domain in sizes and biogenic magnetite in nanoscale. Minor framboidal iron oxides were also  
18 identified, which were previously interpreted as authigenic magnetite that substitutes pyrite.  
19 However, our scanning and transmission electron microscopic (SEM/TEM) observations, along with  
20 optical microscope and Raman spectrum investigations further suggest that these magnetic minerals  
21 are pigmentary hematite and goethite that are incapable of carrying a stable primary magnetization.  
22 We therefore argue that the ChRMs of the limestones from the Zongpu Formation in the Gamba area  
23 are carried by detrital and biogenic magnetites rather than authigenic magnetite. The paleomagnetic  
24 data from the Gamba area are interpreted as primary origin and can thus be used for tectonic  
25 reconstructions. We emphasize that magnetic extraction, integrated with advanced mineralogic  
26 studies (e.g., electron backscatter diffraction and electron diffraction) are effective approaches for  
27 investigating the origin of magnetic carriers in carbonate rocks.

## 28 **1 Introduction**

29 Consecutive indentation of India into continental Asia resulted in a rapid uplift of the Tibetan  
30 Plateau that has profoundly changed the climatic pattern and topography of Asia since the Cenozoic  
31 era (Yin and Harrison, 2000; Jagoutz et al., 2016). The timing and position of the initial collision  
32 between India and Asia remain highly debated (e.g., Ding et al., 2005; Leech et al., 2005; Aitchison

33 et al., 2007; Ali and Aitchison, 2008; Najman et al., 2010; Yi et al., 2011; van Hinsbergen et al.,  
34 2012; Hu et al., 2016; An et al., 2021). On the paleolatitudinal comparison based on reliable  
35 paleomagnetic poles, paleomagnetism provides a direct constrain on timing and locus for the initial  
36 collision between India and Asia (e.g., Dupont-Nivet et al., 2010; Najman et al., 2010; Yi et al.,  
37 2011, 2021)

38 The Indian plate was subjected to rapid northward motion toward Asia during the Cretaceous  
39 and Paleocene (Patriat and Achache, 1984; Yin and Harrison, 2000; van Hinsbergen et al., 2011).  
40 The kinematics of the northern margin of India can be constrained by the Cretaceous and Paleogene  
41 paleomagnetic data obtained from the Tethyan Himalaya (Besse et al., 1984; Patzelt et al., 1996;  
42 Tong et al., 2008; Yi et al., 2011; Yang et al., 2015, 2019; Ma et al., 2016; Meng et al., 2019, 2020;  
43 Y. Zhang et al., 2019; Yuan et al., 2020). For the lack of contemporary volcanic rocks, the Late  
44 Cretaceous to Paleocene sedimentary rocks from the Tethyan Himalaya are especially crucial for  
45 reconstructing the overall process of the India-Asia collision. Several paleomagnetic poles were  
46 reported from the marine sediments of the Tethyan Himalaya with the Late Cretaceous to Paleocene  
47 in ages (Besse et al., 1984; Patzelt et al., 1996; Tong et al., 2008; Yi et al., 2011; Ma et al., 2016;  
48 Yang et al., 2019; Meng et al., 2020; Yuan et al., 2020). In the light of these poles, a variety of  
49 paleogeographic reconstructions were established with small (Besse et al., 1984; Tong et al., 2008),  
50 moderate (Yi et al., 2011), and enlarged (Meng et al., 2020) Greater India or hypothesized oceanic  
51 basins, namely, “Greater India Basin” (van Hinsbergen et al., 2012) or “North India Sea” (Yuan et  
52 al., 2020).

53 A continuously outcropped marine sedimentary sequence is well-preserved in the Gamba area.  
54 Among these units, the Zongshan (71-65 Ma) and Zongpu (62-56 Ma) formations provide a unique  
55 opportunity for constraining the locus of the Tethyan Himalaya covering a critical stage of the India-  
56 Asia collision. Detailed lithological and biostratigraphic (Willems and Zhang, 1993; Wan et al.,  
57 2002a,b), sedimentological (Li et al., 2015), and geochemical (Wang et al., 2008; Q. Zhang et al.,  
58 2019) investigations provide a solid foundation for paleomagnetic studies.

59 Characteristic remanent magnetizations (ChRMs) reported from the Zongshan and Zongpu  
60 formations in the Gamba area passed positive fold and reversal tests, along with internally consistent  
61 magnetostratigraphy and biostratigraphic ages (71-56 Ma), permitting the original authors to interpret  
62 them as primary (Patzelt et al., 1996; Yi et al., 2011). However, based on the detailed rock magnetic  
63 and petrographic studies, along with a reanalysis of the fold test performed on the Zongpu  
64 Formation, Huang et al., (2017a,b) argued for a widespread remagnetization via orogenic fluids in  
65 the Gamba area, and thus the paleomagnetic poles obtained from Zongpu Formation limestones can  
66 no longer be used to constrain the geometry of the India-Asia collision. As a response, Yi et al.  
67 (2017) addressed the reliability of their fold tests performed on the Zongpu and Zongshan formations  
68 and argued for an acquisition of the ChRMs in the early diagenetic stage.

69 On the basis of rock magnetism and SEM observations incorporating EDS analysis, Huang et al.,  
70 (2017a,b, 2019) argued for the presence of abundant authigenic magnetites in carbonates preserved  
71 within the Tethyan domain of Tibet. These authigenic magnetites were suggested to result from a  
72 partial or complete replacement of pyrite crystals/framboids by secondary magnetites that were  
73 responsible for a widespread chemical remagnetization in the Gamba and Tring area, Tethyan  
74 Himalaya (Huang et al., 2017a,b). However, authigenic magnetic minerals are common for marine  
75 sediments due to the diagenesis during the burial process that may alter the combination of magnetic  
76 components (Roberts, 2015 and references therein) and complicate the discrimination of rock  
77 magnetic parameters. The authigenic magnetic spherules cannot be directly related to a chemical

78 remagnetization (Saffer and McCabe, 1992; Suk et al., 1992), although the ability of carrying stable  
79 remanence of these magnetic spherules remains elusive (Xu et al., 1994; Suk and Halgedahl, 1996).  
80 Moreover, as EDS analyses cannot distinguish magnetic particles among magnetite, hematite, and  
81 goethite due to the imprecise measurement of Fe/O ratios (Sun and Jackson, 1994; Xu et al., 1998;  
82 Weil and Van der Voo, 2002; Franke et al., 2007), the arguments by Huang et al., (2017a,b, 2019)  
83 needs to be further studied.

84 In an effort to clarify the type and origin of the magnetic carriers in the Zongpu carbonates, we  
85 carry out a combined study integrating optical microscopy, SEM/TEM observations, and Raman  
86 spectroscopy measurements on thin sections and magnetic extracts of pilot samples from the Zongpu  
87 Formation in the Gamab area, Tethyan Himalaya. By this way, we further evaluated the nature of  
88 ChRMs reported from the Zongpu Formation by previous studies.

## 89 2 Sampling sites and experimental methods

90 Figure 1 illustrates the structure of the Indus-Yarlung Zangbo suture zone, in which  
91 paleomagnetic sampling localities and lithostratigraphic units are indicated. Detailed geological  
92 background is available in many previous studies (e.g., Wan et al., 2002a,b; Yi et al., 2011; Li et al.,  
93 2015; Huang et al., 2017a). The Paleocene carbonate rocks of the Zongpu Formation were deposited  
94 in a shallow-marine carbonate ramp on the northern Indian passive margin (Li et al., 2015). The  
95 Zongpu Formation is divided into four members by lithology; massive limestone (Member I), marls  
96 (Member II), nodular limestones (Member III), and well-bedded limestones (Member IV) (Willems  
97 and Zhang, 1993). Polished thin sections (xg38-3, xg160-1, xg145-3, and xg121-1) were processed  
98 on samples collected by Yi et al. (2011) (red dots in Figure 1C). In addition, **block limestone**  
99 **samples (GB) of ~1 kilogram in weight was collected from the top of the Zongpu Formation**  
100 for a magnetic extraction and SEM/TEM observations (Section A of Yi et al. (2011), Figure 1C).

101 Raman spectra measurements were conducted using a Raman spectrometer (LabRAM HR  
102 Evolution) equipped with a laser (excitation wavelength of 532nm) in the School of Earth and Space  
103 Sciences (SESS), Peking University. Laser power was reduced by a filter to about 1 mW to avoid the  
104 transformation of magnetite, goethite, and pyrite (Hanesch, 2009). Data were obtained with a spectral  
105 resolution of  $1\text{cm}^{-1}$  across the  $100\text{-}1500\text{ cm}^{-1}$  wavenumber offset range. The experiment was carried  
106 out under an objective lens with 100 times magnification. Because of the low laser powers, more than  
107 ninety seconds integration time for individual measurements and 10 accumulations were set to  
108 improve the signal-to-noise ratio. In this study, Raman spectra were provided without smoothing or  
109 fitting to present the original results during the measurements.

110 To further examine the magnetic properties, the carbonate rock samples were first  
111 disaggregated and then put in buffered acetic acid to dissolve ( $\text{pH} = 4$ ) for several days. Magnetic  
112 extraction is performed using a self-designed magnetic probe extraction apparatus (Figure S1A).  
113 The slurry flowed through a tube with dispersed fine magnetic fractions and pumped continuously  
114 through the extraction equipment. Improved extraction-related procedures, following Hounslow et  
115 al. (1999), were used to avoid dissolution effects of ultrafine magnetic particles in samples (Sun and  
116 Jackson,

117 Magnetic extracts of pilot samples were prepared for SEM observation as thin sections using  
118 resin as an adhesive (Figure S1B). An alternative and highly recommended procedure to prepare  
119 SEM samples was to drop the solutions with magnetic extracts on a monocrystalline silicon wafer  
120 (Figure S1C). To prepare TEM specimens, distilled water with magnetic extracts was moved to a

121 small container. A rare-earth magnet hovered ~1 cm above the TEM grid which was floated on the  
122 surface of the solutions, to attract magnetic extracts for ~5 min (Figure S1D). EDS, electron  
123 backscatter diffraction (EBSD), and photographs were performed with SEM/ESEM system at SESS  
124 and Electron Microscopy Laboratory (EML) in the School of Physics, Peking University. The TEM  
125 was performed using a JEOL 2100 TEM (200kV) at the Institute of Geology and Geophysics,  
126 Chinese Academy of Sciences (IGGCAS).

## 127 **3 Results**

### 128 **3.1 Optical petrography and Raman spectroscopy analysis**

129 An analysis of the iron oxide-sulfide assemblages in the thin sections (xg38-3, xg160-1, xg145-  
130 3, and xg121-1) and magnetic extracts (GB) under reflected white light shows that pyrite-substituted  
131 by iron oxides were the most abundant magnetic phase of the Zongpu Formation (Figures 2A-2D, 2I-  
132 2L, and S2). Based on the blood-red internal color under plane-polarized light (Figures 2E-2H, 2M-  
133 2P), we interpret the iron oxides with poor crystallinity as fine-grained pigmentary hematite. Goethite  
134 phases, displaying intense brownish yellow-orange internal reflections, are identified around hematite  
135 pseudoframboids (Figures 2D, 2J-2L). The iron sulfides, inferred as pyrite due to the bright-brassy  
136 colored reflections with a speckly appearance, yielded two morphologic groups: (1) framboid  
137 spherules (Figures 2A, 2B, and 2I) and (2) large euhedral grains (Figures 2C and 2D). The abundant  
138 occurrence of the pigmentary hematite and goethite along calcite boundaries and/or intergranular  
139 dissolved voids are noticeable. In contrast, the extensive presence of pyrite (framboids and euhedral  
140 grains) is well-preserved in calcite crystals as inclusions. Magnetite was not identified by optical  
141 microscope observation probably due to its low concentration, although it was supposed to be the  
142 main magnetic carrier in the limestones of the Zongpu Formation (Yi et al., 2011; Huang et al.,  
143 2017a).

144 Furthermore, the Raman spectrum investigations indicate the presence of hematite, goethite, and  
145 pyrite (Figure 3). These results are consistent with our observations under the optical microscope. As  
146 compared with the corresponding spectra of minerals shown in Hanesch (2009) and the RRUFF  
147 database (<https://rruff.info>), the offset peaks might well be caused by different crystallinities of the  
148 natural minerals.

### 149 **3.2 SEM observations of magnetic extracts**

150 Abundant pure iron oxides were observed from magnetic extracts by SEM observation. These  
151 submicron iron oxide grains are presented in various morphology, consisting of broken-octahedral,  
152 subangular, irregular, and well-rounded crystals (Figures 4A-4J), suggestive of a detrital origin. The  
153 acquired Electron Back-scattering Patterns (EBSPs) for these grains show a spinel pattern (Figures  
154 4M-4P) that confirm a detrital origin for magnetites, although there may be hematite in some cases.  
155 Interestingly, we also found several euhedral magnetic crystals with clear particle boundaries, about  
156 50-100 nm in size (Figures 4K and 4L). Accordingly, we suggest that these submicron and nanoscale  
157 magnetite particles fit the size range of SD and PSD (Dunlop and Özdemir, 1997) and are the  
158 possible remanence carrier in the limestones of the Zongpu Formation in the Gamba area.

159 Despite the frequent occurrence of detrital magnetite, iron oxide spherules were also found in  
160 the magnetic extracts (Figure 4A). EDS line scanning and mapping show that the iron oxide  
161 assemblage contains S in addition to Fe and O in a form of pseudoframboid (Figure 5). Given that  
162 cosmic spherules usually contain a low content of Ni (Brownlow et al., 1966) which was not  
163 detected by the EDS analysis, we exclude the possibility of cosmogenesis. Along with our  
observations in thin

164 sections, we argue that these pseudoframboids are iron (hydr)oxides (hematite and/or goethite) that  
165 substitute framboidal pyrite (Suk et al., 1990).

### 166 3.3 TEM observations of magnetic extracts

167 The TEM observations reveal that magnetic grains with variable grain sizes are commonly  
168 present in magnetic extracts from the Zongpu Formation (Figures 6A-6D). Further high-resolution  
169 TEM (HRTEM) and selected area electron diffraction (SAED) analyses were carried out to determine  
170 the crystal structure of the magnetic particles. All analyzed magnetic minerals, including submicron  
171 and nanosized particles, have clear lattice fringes (Figures 6E and 6F) and sharp diffraction patterns  
172 (Figures 6G-6I) which indicate that the analyzed magnetic minerals are titanomagnetite and  
173 magnetite with well-developed crystallinity.

174 The TEM images revealed presence of both nanosized and euhedral magnetic crystals for the  
175 studied samples (Figures 6C, 6I, and 6L). The grain size of magnetite and titanomagnetite ranges  
176 from tens of nm to several  $\mu\text{m}$ . Non-spheroidal iron oxides are observed in TEM. Together with the  
177 EDS spectra (Figures 6J-6L) and mineral morphologies, we believe that the remanence magnetic  
178 carrier should be detrital magnetite and/or euhedral magnetic particles from the Zongpu Formation in  
179 the Gamba area.

### 180 3.4 Characteristics of demagnetization

181 Previous rock magnetic investigations indicate the main magnetic carriers of remanence are  
182 magnetite from most Zongpu carbonates in the Gamba area, in addition, some of which detected  
183 goethite and hematite (Yi et al., 2011). All specimens were subjected to alternating field (AF)  
184 demagnetization up to 89 mT in the light of their relatively weak natural remnant magnetization  
185 (NRM). Two remnant magnetization components were isolated in the majority of specimens  
186 (Figure 7A-F). After removal of a viscous component, xg0-3, xg38-3, and xg145-2 yield a stable  
187 characteristic remanence (ChRM) (Figure 7A, B, and D). Some specimens reveal an unstable  
188 demagnetization trajectory (xg121-2, and xg160-1; Figure 7C, E, and F) which were discarded for  
189 further discussion (Yi et al., 2011).

## 190 4 Discussion

### 191 4.1 Origin of the euhedral magnetite in nanoscale

192 SD euhedral magnetites were observed in the magnetic extracts (Figures 4K, 4L, and 6C). There  
193 are two possible origins for such magnetic particles in sediments: (1) the magnetic inclusion as  
194 erosional detritus from igneous and metamorphic rocks (e.g., Chang et al., 2016); (2) biogenic  
195 magnetite (Kopp and Kirschvink, 2008). Both types of magnetic particles are able to carry stable  
196 paleomagnetic signals over billions of years (Kirschvink and Lowenstam, 1979; Tarduno et al.,  
197 2006; Tarduno et al., 2010). Usually, most of the magnetic nanoparticle inclusions hosted within  
198 silicate crystals show high content of Si and low content of Ti that can be identified by EDS analyses  
199 (Chang et al., 2016). In this study, however, only very low content of Si and no Ti were detected  
200 from the euhedral magnetic crystals (Figure 6L). Furthermore, silicate minerals (e.g., plagioclase and  
201 clinopyroxene) were not observed in thin sections (Figures 2 and S4), probably due to the low clastic  
202 influx and high carbonate saturation during deposition of the Zongpu Formation (Li et al., 2015). In  
203 this case, the origin of euhedral magnetite in nanoscale from silicate-hosted magnetic mineral  
204 inclusions is highly unlikely. We suggest the nanosized and euhedral magnetic particles are biogenic  
205 magnetite that is capable of carrying stable remanences in limestones (Chang et al., 1987). Further

206 study should be required to detect robust evidence of biogenic magnetite based on a broader  
207 observation of magnetic extracts from Zongpu carbonates in the Gamba area.

#### 208 **4.2 The possible origin of iron oxide spherules**

209 In addition to the detrital and biogenic magnetites observed in magnetic extracts, iron oxide  
210 spherules were also identified from the Zongpu Formation in the Gamba area (Figures 4, 5, and S2).  
211 Several previous studies attribute the remagnetization of carbonates to the replacement of framboidal  
212 pyrite by oxidation that is related to orogenic fluids (see review by McCabe and Elmore, 1989).  
213 However, the photomicrographs of limestone samples in Huang et al. (2017a) and section A of Yi et  
214 al. (2011) present well-preserved fossils (benthic foraminifer, echinoderm, ostracod, and green  
215 algae) with particles/matrix support and show no sign of orogenic-type fluids (Figure S4 and S5; Li  
216 and Hu, 2020). Besides, the variations of carbon and oxygen isotope of bulk carbonate cover the key  
217 interval of the Paleocene-Eocene thermal maximum (PETM) (Q. Zhang et al., 2019). The strontium  
218 isotopic ratios ( $^{87}\text{Sr}/^{86}\text{Sr}$ ) of calcite are comparable with the global oceanic strontium isotope record  
219 (Wang et al., 2008) which indicates that the carbonates in the Gamba area have not been altered by  
220 orogenic fluids. The origin of iron oxide spherules should thus be explained in other mechanisms.

221 Suk et al. (1992) proposed different magnetic mineralogy for the primary and remagnetized  
222 carbonates. The iron sulfides (e.g., pyrite framboids) were moderately or completely oxidized to  
223 hematite in the former while a replacement of magnetite occurs in remagnetized carbonates.  
224 Moreover, oxidation of pyrite under modern atmosphere and groundwater conditions produces  
225 goethite and/or hematite (Todd et al., 2003; Sgavetti et al., 2009; Verron et al., 2019). Recently, a  
226 deep abiotic reaction mechanism of pyrite weathering in rocks was proposed which demonstrated that  
227 fracturing and erosion, in addition to atmospheric oxygen, control the reactivity of iron sulfide  
228 oxidation (Gu et al., 2020). Therefore, we suggest the large amounts of iron (hydr)oxides (e.g.,  
229 goethite and hematite) observed in carbonates from the Zongpu Formation in the Gamba area were  
230 more likely oxidized from pyrite under aqueous solutions in contact with the atmosphere.

#### 231 **4.3 Primary versus secondary origin of the ChRMs**

232 The secondary superparamagnetic (SP) to stable single domain (SSD) grain-sized magnetite is a  
233 general indicator for chemical remagnetization in carbonates which could well explain the  
234 remagnetization that occurred in the Paleozoic carbonates of North America (Channell and McCabe,  
235 1994; Suk and Halgedahl, 1996; Xu et al., 1998; Elmore et al., 2006). A mix of SP and SD particles  
236 yields wasp-waisted hysteresis loops and distribution of Day plot along the SP-SD mixing line  
237 (Jackson and Swanson-Hysell, 2012). Nevertheless, magnetic minerals in different assemblage and  
238 shape anisotropy can also present contrasting coercivity distributions, resulting in wasp-waisted  
239 hysteresis loops (Jackson, 1990; Roberts et al., 1995; Newell and Merrill, 2000; Zwing et al., 2005;  
240 Jackson and Swanson-Hysell, 2012). It is generally difficult to interpret the magnetic grain size and  
241 mineralogy by wasp-waisted hysteresis loops or Day-plot only (Tauxe et al., 1996; Roberts et al.,  
242 2018). It also should be caution when using a Day diagram to diagnose remagnetization as  
243 occasionally ‘false positives’ and ‘false negatives’ results may present (Jackson and Swanson-Hysell,  
244 2012; Roberts et al., 2018). Moreover, the validity of application of Day-plot in shallow-water  
245 carbonates, which are isolated from aqueous detrital input, remains unverified (Jackson and  
246 Swanson-Hysell, 2012). On the other hand, our SEM/TEM observations indicate the content of  
247 abundant detrital and biogenic magnetites in the investigated carbonates (Figures 4 and 6). The  
248 optical petrography and Raman spectra analyses present robust evidence that iron (hydr)oxides, i.e.,  
249 goethite and hematite (Figures 2, 3, and S2), rather than magnetite, as substitutes of pyrite framboids.  
250 The imaginable detrital and biogenic magnetite, along with goethite and hematite, would yield wasp-

251 wasted hysteresis loops and distribution of Day plot along the SP-SD mixing line which leads to an  
252 incorrect interpretation of remagnetization from Day plot locations (Huang et al., 2017a,b, 2019).

253 The argument of previous paleomagnetic investigation for a chemical remagnetization of the  
254 carbonate rocks in the Gamba area was mainly based on SEM and EDS interpretation (Huang et al.,  
255 2017a). Whereafter, the same authors performed analogous analytical processes on the Upper  
256 Cretaceous to Paleocene carbonates from the Tingri area in the Tethyan Himalaya and the Upper  
257 Triassic limestones in the eastern Qiangtang block, argued for a widespread remagnetization in the  
258 Tibetan Tethyan domain (Huang et al., 2017b, 2019). However, the critical “authigenic magnetite”,  
259 along with the “orogenic fluids” are only speculated by the authors, regardless that conventional EDS  
260 techniques only have a semi-quantitative character which cannot directly distinguish the exact iron  
261 oxides. On the contrary, the geochemical evidence from the Zongpu Formation precludes the  
262 existence of widespread orogenic fluids as discussed above. Consequently, the remagnetization  
263 mechanism of chemical alteration suggested by Huang et al. (2017a) is problematic.

264 The presence of abundant detrital and biogenic magnetites in the Zongpu limestones precludes  
265 widespread chemical remagnetization in the Gamba area. The rock magnetic investigations (Yi et al.,  
266 2011; Huang et al., 2017a) and the characteristics of demagnetization (Figure 7) are consistent with  
267 high-resolution petrographic observations (Figures 2, 4, and 6). On the other hand, the occurrence of  
268 anatase in the underlying Jidula Formation suggests that the overlying Zongpu limestones were never  
269 heated over 260°C (Patzelt et al., 1996) and hence exclude a thermal remagnetization in the Gamba  
270 area. Moreover, the ChRMs from Gamba carbonates yielded positive fold and reversal tests (Patzelt  
271 et al., 1996; Yi et al., 2011, 2017), and the paleomagnetic pole from the Zongpu Formation hence  
272 meets all the criteria for a paleomagnetic study ( $R = 7$ ) (Meert et al., 2020). We therefore concluded  
273 that detrital and biogenic magnetites are the main magnetic carriers of primary remanence and the  
274 paleomagnetic results reported by Yi et al. (2011) from the Gamba area can still be used for  
275 paleogeographic reconstruction.

## 276 **5 Conclusion and perspective**

277 The high-resolution petrographic study was carried out on Paleocene carbonates (the Zongpu  
278 Formation) from Gamba, South Tibet. Electron microscopic observation of magnetic extracts  
279 identified abundant detrital and biogenic magnetites. Minor framboidal iron oxides were also  
280 identified using SEM, optical microscope, and Raman spectrum investigations. However, the  
281 magnetic minerals in these framboids are pigmentary hematite and/or goethite rather than authigenic  
282 magnetite. Therefore, the ChRMs of the limestones from the Zongpu Formation in the Gamba area  
283 are carried by detrital and biogenic magnetites. The arguments of chemical remagnetization, based  
284 on oversimplified semiquantitative EDS analyses and incomplete rock magnetic measurements in  
285 previous studies, should be rejected. Instead, the paleomagnetic data obtained from the Paleocene  
286 carbonates in the Gamba area can be used for tectonic reconstructions. We suggest that  
287 comprehensive analyses of magnetic extracts with advanced EBSD and TEM are extremely  
288 important and favorable to diagnose the substantial magnetization carriers in carbonate rocks. The  
289 remagnetization hypotheses in Paleocene carbonates from the Tingri area, Tethyan Himalaya, and the  
290 Late Triassic carbonates from the Qiangtang terrane require further study based on the thorough  
291 petrographic and mineralogical investigations to determine the origin of the magnetization.

## 292 **6 Funding**

293 This study was supported by grants from the National Natural Science Foundation of China (Grants  
294 No. 92055205, 41888101) and the Second Tibetan Plateau Scientific Expedition and Research  
295 Program (STEP; Grant No. 2019QZKK0703).

## 296 **7 Acknowledgments**

297 We are grateful to Xu Tang at the Electron Microscopy Laboratory, IGGCAS for helping with TEM  
298 operation and David Richard and Richard T. Wilkin for helpful discussions.

## 299 **1 References**

- 300 Aitchison, J.C., Ali, J.R., and Davis, A.M. (2007). When and where did India and Asia collide?  
301 *Journal of Geophysical Research* 112(B5). doi: 10.1029/2006jb004706.
- 302 Ali, J.R., and Aitchison, J.C. (2008). Gondwana to Asia: Plate tectonics, paleogeography and the  
303 biological connectivity of the Indian sub-continent from the Middle Jurassic through latest  
304 Eocene (166–35Ma). *Earth-Science Reviews* 88, 145-166. doi:  
305 10.1016/j.earscirev.2008.01.007.
- 306 An, W., Hu, X., Garzanti, E., Wang, J.G., and Liu, Q. (2021). New Precise Dating of the India - Asia  
307 Collision in the Tibetan Himalaya at 61 Ma. *Geophysical Research Letters* 48(3). doi:  
308 10.1029/2020gl090641.
- 309 Besse, J., Courtillot, V., Pozzi, J., Westphal, M., and Zhou, Y. (1984). Palaeomagnetic estimates of  
310 crustal shortening in the Himalayan thrusts and Zangbo suture. *Nature* 311(5987), 621-626.  
311 doi: 10.1038/311621a0.
- 312 Brownlow, A.E., Hunter, W., and Parkin, D.W. (1966). Cosmic Spherules in a Pacific Core.  
313 *Geophysical Journal International* 12(1), 1-13. doi: 10.1111/j.1365-246X.1966.tb03096.x.
- 314 Chang, L., Roberts, A.P., Heslop, D., Hayashida, A., Li, J., Zhao, X., et al. (2016). Widespread  
315 occurrence of silicate - hosted magnetic mineral inclusions in marine sediments and their  
316 contribution to paleomagnetic recording. *Journal of Geophysical Research: Solid Earth* 121,  
317 8415-8431. doi: 10.1002/2016JB013109.
- 318 Chang, S., Kirschvink, J.L., and Stolz, J.F. (1987). Biogenic magnetite as a primary remanence  
319 carrier in limestone deposits. *Physics of the Earth and Planetary Interiors* 46(1-3), 289-303.  
320 doi: 10.1016/0031-9201(87)90191-9.
- 321 Channell, J.E.T., and McCabe, C. (1994). Comparison of magnetic hysteresis parameters of  
322 unremagnetized and remagnetized limestones. *Journal of Geophysical Research: Solid Earth*  
323 99(B3), 4613-4623. doi: 10.1029/93JB02578.
- 324 Ding, L., Kapp, P., and Wan, X. (2005). Paleocene - Eocene record of ophiolite obduction and initial  
325 India - Asia collision, south central Tibet. *Tectonics* 24(3). doi: 10.1029/2004TC001729.
- 326 Dunlop, D.J., and Özdemir, Ö. (1997). *Rock magnetism: fundamentals and frontiers*. Cambridge  
327 university press.



- 328 Dupont-Nivet, G., Lippert, P.C., Van Hinsbergen, D.J.J., Meijers, M.J.M., and Kapp, P. (2010).  
329 Palaeolatitude and age of the Indo-Asia collision: palaeomagnetic constraints. *Geophysical*  
330 *Journal International* 182(3), 1189-1198. doi: 10.1111/j.1365-246X.2010.04697.x.
- 331 Elmore, R.D., Lee-Egger Foucher, J., Evans, M., Lewchuk, M., and Cox, E. (2006). Remagnetization  
332 of the Tonoloway Formation and the Helderberg Group in the Central Appalachians: testing  
333 the origin of syntilting magnetizations. *Geophysical Journal International* 166(3), 1062-1076.  
334 doi: 10.1111/j.1365-246X.2006.02875.x.
- 335 Franke, C., Pennock, G., Drury, M.R., Engelmann, R., Lattard, D., Garming, J.F.L., et al. (2007).  
336 Identification of magnetic Fe-Ti oxides in marine sediments by electron backscatter  
337 diffraction in scanning electron microscopy. *Geophysical Journal International* 170(2), 545-  
338 555. doi: 10.1111/j.1365-246X.2007.03410.x.
- 339 Gu, X., Heaney, P.J., Reis, F.D.A., and Brantley, S.L. (2020). Deep abiotic weathering of pyrite.  
340 *Science* 370(6515). doi: 10.1126/science.abb8092.
- 341 Hanesch, M. (2009). Raman spectroscopy of iron oxides and (oxy) hydroxides at low laser power and  
342 possible applications in environmental magnetic studies. *Geophysical Journal International*  
343 177(3), 941-948. doi: 10.1111/j.1365-246X.2009.04122.x.
- 344 Hounslow, M.W., Maher, B.A., Walden, J., Oldfield, F., and Smith, J. (1999). Laboratory procedures  
345 for quantitative extraction and analysis of magnetic minerals from sediments. *Environmental*  
346 *Magnetism, A Practical Guide. Quaternary Research Association, Technical Guide 6*, 139-  
347 164.
- 348 Hu, X., Garzanti, E., Wang, J., Huang, W., An, W., and Webb, A. (2016). The timing of India-Asia  
349 collision onset—Facts, theories, controversies. *Earth-Science Reviews* 160, 264-299. doi:  
350 10.1016/j.earscirev.2016.07.014.
- 351 Huang, W., Jackson, M.J., Dekkers, M.J., Zhang, Y., Zhang, B., Guo, Z., et al. (2019). Challenges in  
352 isolating primary remanent magnetization from Tethyan carbonate rocks on the Tibetan  
353 Plateau: Insight from remagnetized Upper Triassic limestones in the eastern Qiangtang block.  
354 *Earth and Planetary Science Letters* 523, 115695. doi: 10.1016/j.epsl.2019.06.035.
- 355 Huang, W., Lippert, P.C., Jackson, M.J., Dekkers, M.J., Zhang, Y., Li, J., et al. (2017a).  
356 Remagnetization of the Paleogene Tibetan Himalayan carbonate rocks in the Gamba area:  
357 Implications for reconstructing the lower plate in the India-Asia collision. *Journal of*  
358 *Geophysical Research-Solid Earth* 122(2), 808-825. doi: 10.1002/2016jb013662.
- 359 Huang, W., Lippert, P.C., Zhang, Y., Jackson, M.J., Dekkers, M.J., Li, J., et al. (2017b).  
360 Remagnetization of carbonate rocks in southern Tibet: Perspectives from rock magnetic and  
361 petrographic investigations. *Journal of Geophysical Research: Solid Earth* 122(4), 2434-  
362 2456. doi: 10.1002/2017jb013987.
- 363 Jackson, M. (1990). Diagenetic sources of stable remanence in remagnetized Paleozoic cratonic  
364 carbonates: A rock magnetic study. *Journal of Geophysical Research: Solid Earth* 95(B3),  
365 2753-2761. doi: 10.1029/JB095iB03p02753.

- 366 Jackson, M., and Swanson-Hysell, N.L. (2012). Rock magnetism of remagnetized carbonate rocks:  
367 Another look. *Geological Society, London, Special Publications* 371(1), 229-251. doi:  
368 10.1144/SP371.3.
- 369 Jagoutz, O., Macdonald, F.A., and Royden, L. (2016). Low-latitude arc–continent collision as a  
370 driver for global cooling. *Proceedings of the National Academy of Sciences* 113(18), 4935-  
371 4940. doi: 10.1073/pnas.1523667113.
- 372 Kirschvink, J.L., and Lowenstam, H.A. (1979). Mineralization and magnetization of chiton teeth:  
373 paleomagnetic, sedimentologic, and biologic implications of organic magnetite. *Earth and*  
374 *Planetary Science Letters* 44(2), 193-204. doi: 10.1016/0012-821X(79)90168-7.
- 375 Kopp, R.E., and Kirschvink, J.L. (2008). The identification and biogeochemical interpretation of  
376 fossil magnetotactic bacteria. *Earth-Science Reviews* 86(1), 42-61. doi:  
377 10.1016/j.earscirev.2007.08.001.
- 378 Leech, M.L., Singh, S., Jain, A., Klemperer, S.L., and Manickavasagam, R. (2005). The onset of  
379 India–Asia continental collision: early, steep subduction required by the timing of UHP  
380 metamorphism in the western Himalaya. *Earth and Planetary Science Letters* 234(1-2), 83-  
381 97. doi: 10.1016/j.epsl.2005.02.038.
- 382 Li, J., and Hu, X. (2020). A photomicrograph dataset of Late Cretaceous to Early Paleogene  
383 carbonate rocks in Tibetan Himalaya. *China Scientific Data* 5. doi:  
384 10.11922/csdata.2020.0072.zh.
- 385 Li, J., Hu, X., Garzanti, E., An, W., and Wang, J. (2015). Paleogene carbonate microfacies and  
386 sandstone provenance (Gamba area, South Tibet): Stratigraphic response to initial India–Asia  
387 continental collision. *Journal of Asian Earth Sciences* 104, 39-54. doi:  
388 10.1016/j.jseaes.2014.10.027.
- 389 Ma, Y., Yang, T., Bian, W., Jin, J., Zhang, S., Wu, H., et al. (2016). Early Cretaceous paleomagnetic  
390 and geochronologic results from the Tethyan Himalaya: Insights into the Neotethyan  
391 paleogeography and the India-Asia collision. *Sci Rep* 6, 21605. doi: 10.1038/srep21605.
- 392 McCabe, C., and Elmore, R.D.J.R.o.G. (1989). The occurrence and origin of late Paleozoic  
393 remagnetization in the sedimentary rocks of North America. 27(4), 471-494.
- 394 Meert, J.G., Pivarunas, A.F., Evans, D., Pisarevsky, S.A., and Salminen, J.M. (2020). The  
395 magnificent seven: A proposal for modest revision of the quality index. *Tectonophysics*  
396 790(5), 228549. doi: 10.1016/j.tecto.2020.228549.
- 397 Meng, J., Gilder, S.A., Wang, C., Coe, R.S., Tan, X., Zhao, X., et al. (2019). Defining the Limits of  
398 Greater India. *Geophysical Research Letters*. doi: 10.1029/2019gl082119.
- 399 Meng, J., Lhuillier, F., Wang, C., Liu, H., Eid, B., and Li, Y. (2020). Paleomagnetism of Paleocene -  
400 Maastrichtian (60 - 70 Ma) Lava Flows From Tian Shan (Central Asia): Directional Analysis  
401 and Paleointensities. *Journal of Geophysical Research: Solid Earth* 125(9), e2019JB018631.  
402 doi: 10.1029/2019JB018631.

- 403 Najman, Y., Appel, E., Boudagher-Fadel, M., Bown, P., Carter, A., Garzanti, E., et al. (2010).  
404 Timing of India-Asia collision: Geological, biostratigraphic, and palaeomagnetic constraints.  
405 *Journal of Geophysical Research* 115(B12). doi: 10.1029/2010jb007673.
- 406 Newell, A.J., and Merrill, R.T. (2000). Size dependence of hysteresis properties of small pseudo -  
407 single - domain grains. *Journal of Geophysical Research: Solid Earth* 105(B8), 19393-  
408 19403. doi: 10.1029/2000JB900122.
- 409 Patriat, P., and Achache, J. (1984). India-Eurasia collision chronology has implications for crust  
410 shortening and diving mechanism of plates. *Nature* 311(18), 615-621. doi: 10.1038/311615a0
- 411 Patzelt, A., Li, H., Wang, J., and Appel, E. (1996). Palaeomagnetism of Cretaceous to Tertiary  
412 sediments from southern Tibet: evidence for the extent of the northern margin of India prior  
413 to the collision with Eurasia. *Tectonophysics* 259(4), 259-284. doi: 10.1016/0040-  
414 1951(95)00181-6.
- 415 Roberts, A.P., Cui, Y., and Verosub, K.L. (1995). Wasp - waisted hysteresis loops: Mineral magnetic  
416 characteristics and discrimination of components in mixed magnetic systems. *Journal of*  
417 *Geophysical Research: Solid Earth* 100(B9), 17909-17924. doi: 10.1029/95JB00672.
- 418 Roberts, A.P., Tauxe, L., Heslop, D., Zhao, X., and Jiang, Z. (2018). A Critical Appraisal of the  
419 “Day” Diagram. *Journal of Geophysical Research: Solid Earth* 123(4), 2618-2644. doi:  
420 10.1002/2017JB015247.
- 421 Saffer, B., and McCabe, C. (1992). Further studies of carbonate remagnetization in the northern  
422 Appalachian basin. *Journal of Geophysical Research: Solid Earth* 97(B4), 4331-4348. doi:  
423 10.1029/91JB02746.
- 424 Sgavetti, M., Pompilio, L., Roveri, M., Manzi, V., Valentino, G., Lugli, S., et al. (2009). Two  
425 geologic systems providing terrestrial analogues for the exploration of sulfate deposits on  
426 Mars: Initial spectral characterization. *Planetary and Space Science* 57(5-6), 614-627. doi:  
427 10.1016/j.pss.2008.05.010.
- 428 Suk, D., and Halgedahl, S.L. (1996). Hysteresis properties of magnetic spherules and whole rock  
429 specimens from some Paleozoic platform carbonate rocks. *Journal of Geophysical Research:*  
430 *Solid Earth* 101(B11), 25053-25075. doi: 10.1029/96JB02271.
- 431 Suk, D., Peacor, D., and Van der Voo, R. (1990). Replacement of pyrite framboids by magnetite in  
432 limestone and implications for palaeomagnetism. *Nature* 345(6276), 611-613. doi:  
433 10.1038/345611a0.
- 434 Suk, D., Van der Voo, R., and Peacor, D.R. (1992). SEM/STEM observation of magnetic minerals in  
435 presumably unremagnetized Paleozoic carbonates from Indiana and Alabama. *Tectonophysics*  
436 215(3-4), 255-272. doi: 10.1016/0040-1951(92)90356-B.
- 437 Sun, W., and Jackson, M. (1994). Scanning electron microscopy and rock magnetic studies of  
438 magnetic carriers in remagnetized early Paleozoic carbonates from Missouri. *Journal of*  
439 *Geophysical Research: Solid Earth* 99(B2), 2935-2942. doi: 10.1029/93JB02761.

- 440 Tarduno, J.A., Cottrell, R.D., and Smirnov, A.V. (2006). The paleomagnetism of single silicate  
441 crystals: Recording geomagnetic field strength during mixed polarity intervals, superchrons,  
442 and inner core growth. *Reviews of Geophysics* 44(1), RG1002. doi: 10.1029/2005RG000189.
- 443 Tarduno, J.A., Cottrell, R.D., Watkeys, M.K., Hofmann, A., Doubrovine, P.V., Mamajek, E.E., et al.  
444 (2010). Geodynamo, Solar Wind, and Magnetopause 3.4 to 3.45 Billion Years Ago. *Science*  
445 327(5970), 1238-1240. doi: 10.1126/science.1183445.
- 446 Tauxe, L., Mullender, T., and Pick, T. (1996). Potbellies, wasp - waists, and superparamagnetism in  
447 magnetic hysteresis. *Journal of Geophysical Research: Solid Earth* 101(B1), 571-583.
- 448 Todd, E.C., Sherman, D.M., and Purton, J.A. (2003). Surface oxidation of pyrite under ambient  
449 atmospheric and aqueous (pH= 2 to 10) conditions: electronic structure and mineralogy from  
450 X-ray absorption spectroscopy. *Geochimica et Cosmochimica Acta* 67(5), 881-893. doi:  
451 10.1016/S0016-7037(02)00957-2.
- 452 Tong, Y., Yang, Z., Zheng, L., Yang, T., Shi, L., Sun, Z., et al. (2008). Early Paleocene  
453 paleomagnetic results from southern Tibet, and tectonic implications. *International Geology*  
454 *Review* 50(6), 546-562. doi: 10.2747/0020-6814.50.6.546
- 455 van Hinsbergen, D.J.J., Lippert, P.C., Dupont-Nivet, G., McQuarrie, N., Doubrovine, P.V., Spakman,  
456 W., et al. (2012). Greater India Basin hypothesis and a two-stage Cenozoic collision between  
457 India and Asia. *Proceedings of the National Academy of Sciences* 109(20), 7659-7664. doi:  
458 10.1073/pnas.1117262109.
- 459 van Hinsbergen, D.J.J., Steinberger, B., Doubrovine, P.V., and Gassmüller, R. (2011). Acceleration  
460 and deceleration of India-Asia convergence since the Cretaceous: Roles of mantle plumes and  
461 continental collision. *Journal of Geophysical Research* 116(B6). doi: 10.1029/2010jb008051.
- 462 Verron, H., Sterpenich, J., Bonnet, J., Bourdelle, F., Mosser-Ruck, R., Lorgeoux, C., et al. (2019).  
463 Experimental study of pyrite oxidation at 100° C: implications for deep geological radwaste  
464 repository in claystone. *Minerals* 9(7), 427. doi: 10.3390/min9070427.
- 465 Wan, X., Jansa, L.F., and Sarti, M. (2002a). Cretaceous and Paleogene boundary strata in southern  
466 Tibet and their implication for the India - Eurasia collision. *Lethaia* 35(2), 131-146. doi:  
467 10.1080/002411602320183999.
- 468 Wan, X., Liang, D., and Li, G. (2002b). Palaeocene strata in Gamba, Tibet and influence of  
469 tectonism. *Acta Geologica Sinica* 76(2), 155-162. doi: 10.3321/j.issn:0001-5717.2002.02.002
- 470 Wang, X., Wan, X., and Li, G. (2008). Late Cretaceous to early Paleogene strontium isotopic  
471 stratigraphy in the Gamba area, Tibet. *Geology in China* 4, 598-607. doi: 10.3969/j.issn.1000-  
472 3657.2008.04.004
- 473 Weil, A.B., and Van der Voo, R. (2002). Insights into the mechanism for orogen - related carbonate  
474 remagnetization from growth of authigenic Fe - oxide: A scanning electron microscopy and  
475 rock magnetic study of Devonian carbonates from northern Spain. *Journal of Geophysical*  
476 *Research: Solid Earth* 107(B4), EPM 1-1-EPM 1-14. doi: 10.1029/2001JB000200.

- 477 Willems, H., and Zhang, B. (1993). Cretaceous and lower Tertiary sediments of the Tibetan Tethys  
478 Himalaya in the area of Tingri (South Tibet, PR China). *Geoscientific Investigation in the*  
479 *Tethyan Himalayas. Berichte aus dem Fachbereich Geowissenschaften der Universität*  
480 *Bremen* 38, 28-47.
- 481 Xu, W., Van der Voo, R., and Peacor, D.R. (1994). Are magnetite spherules capable of carrying  
482 stable magnetizations? *Geophysical Research letters* 21(7), 517-520. doi:  
483 10.1029/94GL00366.
- 484 Xu, W., Van der Voo, R., and Peacor, D.R. (1998). Electron microscopic and rock magnetic study of  
485 remagnetized Leadville carbonates, central Colorado. *Tectonophysics* 296(3-4), 333-362. doi:  
486 10.1016/S0040-1951(98)00146-2.
- 487 Yang, T., Jin, J., Bian, W., Ma, Y., Gao, F., Peng, W., et al. (2019). Precollisional Latitude of the  
488 Northern Tethyan Himalaya From the Paleocene Redbeds and Its Implication for Greater  
489 India and the India-Asia collision. *Journal of Geophysical Research: Solid Earth* 124(11),  
490 10777-10798. doi: 10.1029/2019JB017927.
- 491 Yang, T., Ma, Y., Bian, W., Jin, J., Zhang, S., Wu, H., et al. (2015). Paleomagnetic results from the  
492 Early Cretaceous Lakang Formation lavas: Constraints on the paleolatitude of the Tethyan  
493 Himalaya and the India-Asia collision. *Earth and Planetary Science Letters* 428, 120-133.  
494 doi: 10.1016/j.epsl.2015.07.040.
- 495 Yi, Z., Appel, E., and Huang, B. (2017). Comment on "Remagnetization of the Paleogene Tibetan  
496 Himalayan carbonate rocks in the Gamba area: Implications for reconstructing the lower plate  
497 in the India-Asia collision" by Huang et al. *Journal of Geophysical Research-Solid Earth*  
498 122(7), 4852-4858. doi: 10.1002/2017jb014353.
- 499 Yi, Z., Huang, B., Chen, J., Chen, L., and Wang, H. (2011). Paleomagnetism of early Paleogene  
500 marine sediments in southern Tibet, China: Implications to onset of the India-Asia collision  
501 and size of Greater India. *Earth and Planetary Science Letters* 309(1-2), 153-165. doi:  
502 10.1016/j.epsl.2011.07.001.
- 503 Yi, Z., Wang, T., Meert, J.G., Zhao, Q., and Liu, Y. (2021). An Initial Collision of India and Asia in  
504 the Equatorial Humid Belt. *Geophysical Research Letters* 48(9), e2021GL093408. doi:  
505 10.1029/2021GL093408.
- 506 Yin, A., and Harrison, T.M. (2000). Geologic evolution of the Himalayan-Tibetan orogen. *Annual*  
507 *Review of Earth and Planetary Sciences* 28(1), 211-280. doi: 10.1146/annurev.earth.28.1.211.
- 508 Yuan, J., Yang, Z., Deng, C., Krijgsman, W., Hu, X., Li, S., et al. (2020). Rapid drift of the Tethyan  
509 Himalaya terrane before two-stage India-Asia collision. *National Science Review*. doi:  
510 10.1093/nsr/nwaa173.
- 511 Zhang, Q., Willems, H., Ding, L., and Xu, X. (2019a). Response of larger benthic foraminifera to the  
512 Paleocene-Eocene thermal maximum and the position of the Paleocene/Eocene boundary in  
513 the Tethyan shallow benthic zones: Evidence from south Tibet. *Geological Society of*  
514 *America Bulletin* 131(1-2), 84-98. doi: 10.1130/B31813.1.

515 Zhang, Y., Huang, B.C., and Zhao, Q. (2019b). New paleomagnetic positive proof of the rigid or  
516 quasi-rigid Greater Indian Plate during the Early Cretaceous. *Chinese Science Bulletin* 64(21),  
517 2225-2244. doi: 10.1360/n972019-00196.

518 Zwing, A., Matzka, J., Bachtadse, V., and Soffel, H. (2005). Rock magnetic properties of  
519 remagnetized Palaeozoic clastic and carbonate rocks from the NE Rhenish massif, Germany.  
520 *Geophysical Journal International* 160(2), 477-486. doi: 10.1111/j.1365-246X.2004.02493.x.

## 521 2 Figure captions

522 **Figure 1.** (A) Schematic structural map of the India-Asia collision zone. (B) Geologic map of the Gamba area  
523 with the sampling locations of Yi et al. (2011) (red star) and Huang et al., (2017a) (green star). (C)  
524 Lithostratigraphy of section A of Yi et al. (2011). Red and blue dots indicate the sampling levels for samples  
525 collected for thin sections observation and magnetic extraction, respectively.

526 **Figure 2.** Photomicrographs illustrating the iron oxide mineralogical features of limestones from the Zongpu  
527 Formation in the Gamba area under reflected light (A-D, I-L) and plane-polarized light (E-H, M-P) images.  
528 **White dots in Figures 2C and 2L represent the spots of Raman spectroscopy analyses in Figure 3.** Cal =  
529 calcite; Gt = goethite; pHem = **pigmentary** hematite; Py = pyrite.

530 **Figure 3.** Raman spectrum of the limestones from the Zongpu Formation. Three types of Fe-O-S minerals,  
531 i.e., hematite ( $222\text{ cm}^{-1}$ ,  $297\text{ cm}^{-1}$ , and  $390\text{ cm}^{-1}$ ) (A), goethite ( $208\text{ cm}^{-1}$ ,  $270\text{ cm}^{-1}$  and  $380\text{ cm}^{-1}$ ) (B) and pyrite  
532 ( $344\text{ cm}^{-1}$  and  $379\text{ cm}^{-1}$ ) (C) can be identified in the Raman spectra.

533 **Figure 4.** (A-L) Secondary-electron SEM images of magnetic extracts in limestones of the Zongpu Formation.  
534 (M and P) EBSPs solution of iron oxides corresponding to the white circles indicated in Figure 4 A-C. Zone  
535 axes are labeled using Miller indices. Note the white circle areas are not as accurate as that was shown in the  
536 images, because of the low resolution of SEM during EBSD analyses. White arrows in Figures 4K and 4L  
537 indicate the possible occurrence of biogenic magnetite. White dots represent the EDS spots as shown in Figure  
538 S3. [Fe-O] = iron oxides; **Mag = magnetite.**

539 **Figure 5.** Elemental mapping exhibits elemental compositions and distributions of an iron-oxidized framboid.  
540 (A) SEM image of a framboid with line scan by energy spectrum. (B-D) Fe, S, and O elements are scattered in  
541 most areas. White arrows show significant variation in the distributions of Fe, O, and S elements.

542 **Figure 6.** High-resolution TEM and SAED analyses of magnetic minerals for magnetic extracts from  
543 limestones in the Zongpu Formation. (A-D) Bright-field TEM images at progressively higher magnifications  
544 reveal characteristics of mixed magnetic particles with different sizes. (E-F) Clear lattice fringes for the  
545 magnetic minerals are observed. **The lattice fringes in (F) correspond to  $\langle 311 \rangle$  plane of titanomagnetite.** (G-I)  
546 **Ring-like and spot-like SAED patterns indicate the particle aggregate and single particle, respectively. The**  
547 **corresponding Miller indices (hkl) are illustrated.** (J-L) EDS spectra of the magnetic particles in B-D. The  
548 particles in different sizes are magnetite (B, C) and titanomagnetite (D).

549 **Figure 7.** Orthogonal (Zijderveld) vector plots of specimens from Yi et al. (2011) corresponding to  
550 the samples of magnetic extraction and thin sections. Directions are plotted in-situ; solid and open  
551 circles represent vector endpoints projected onto horizontal and vertical planes, respectively.

552

553

554

In review

Figure 1.JPEG

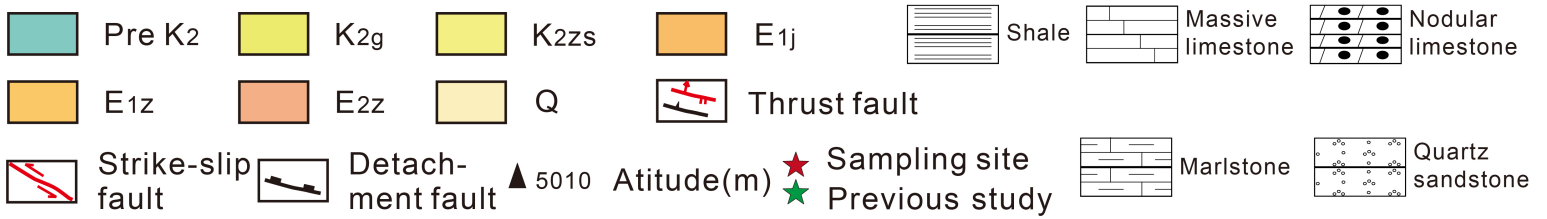
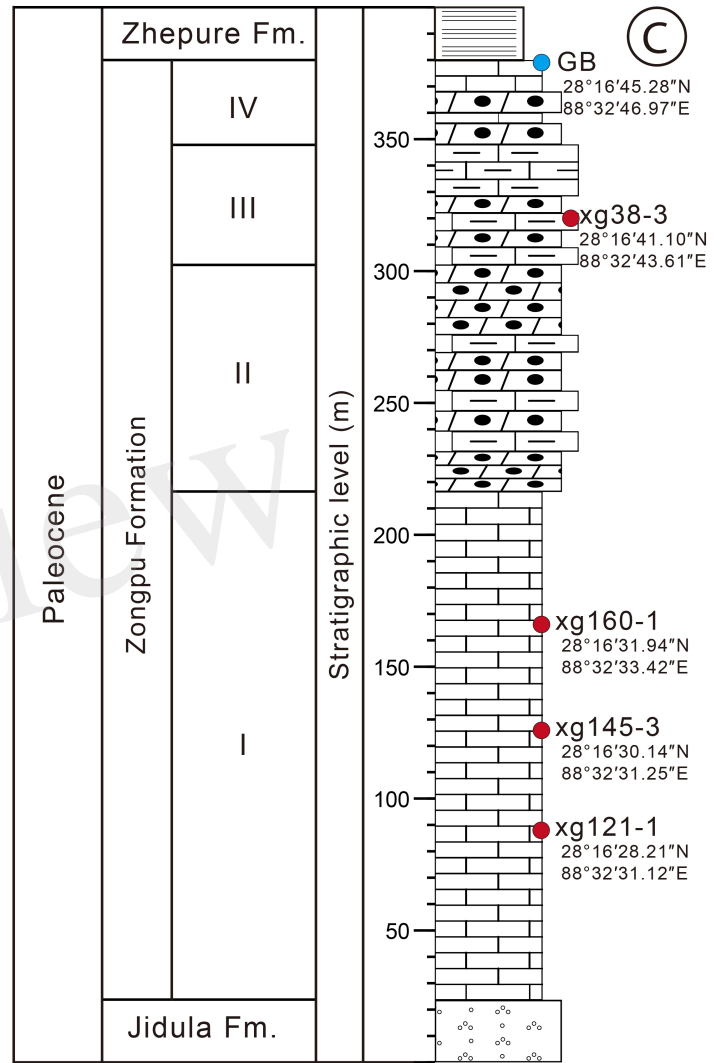
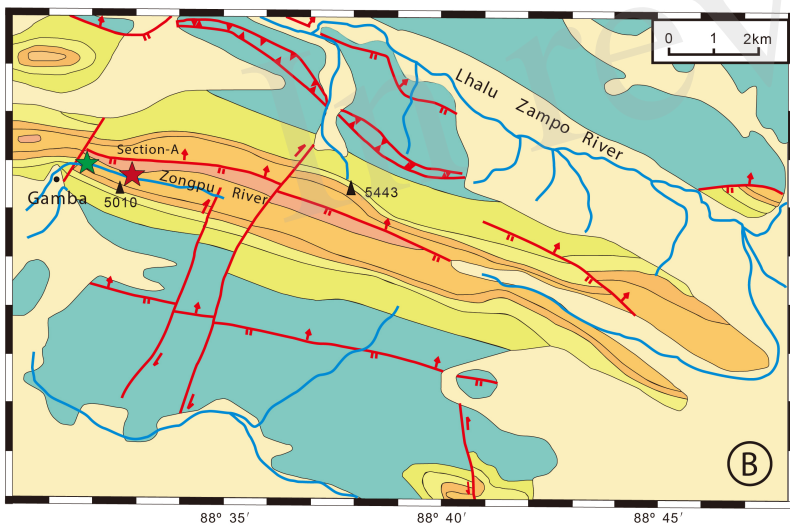
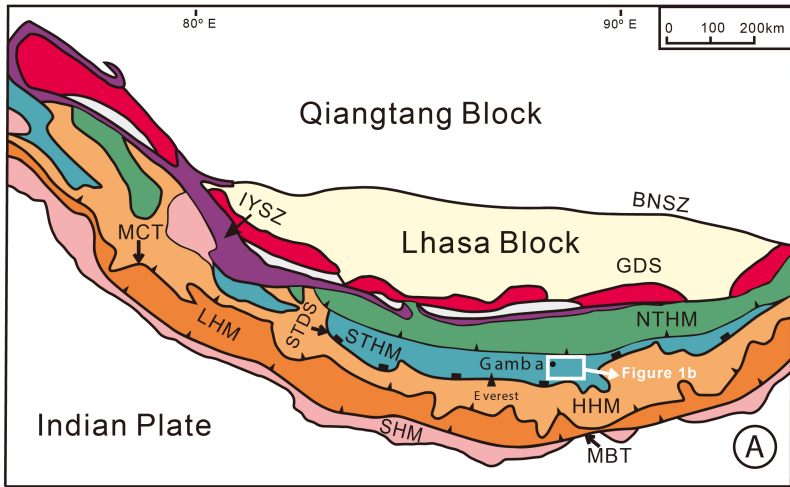




Figure 2.JPEG

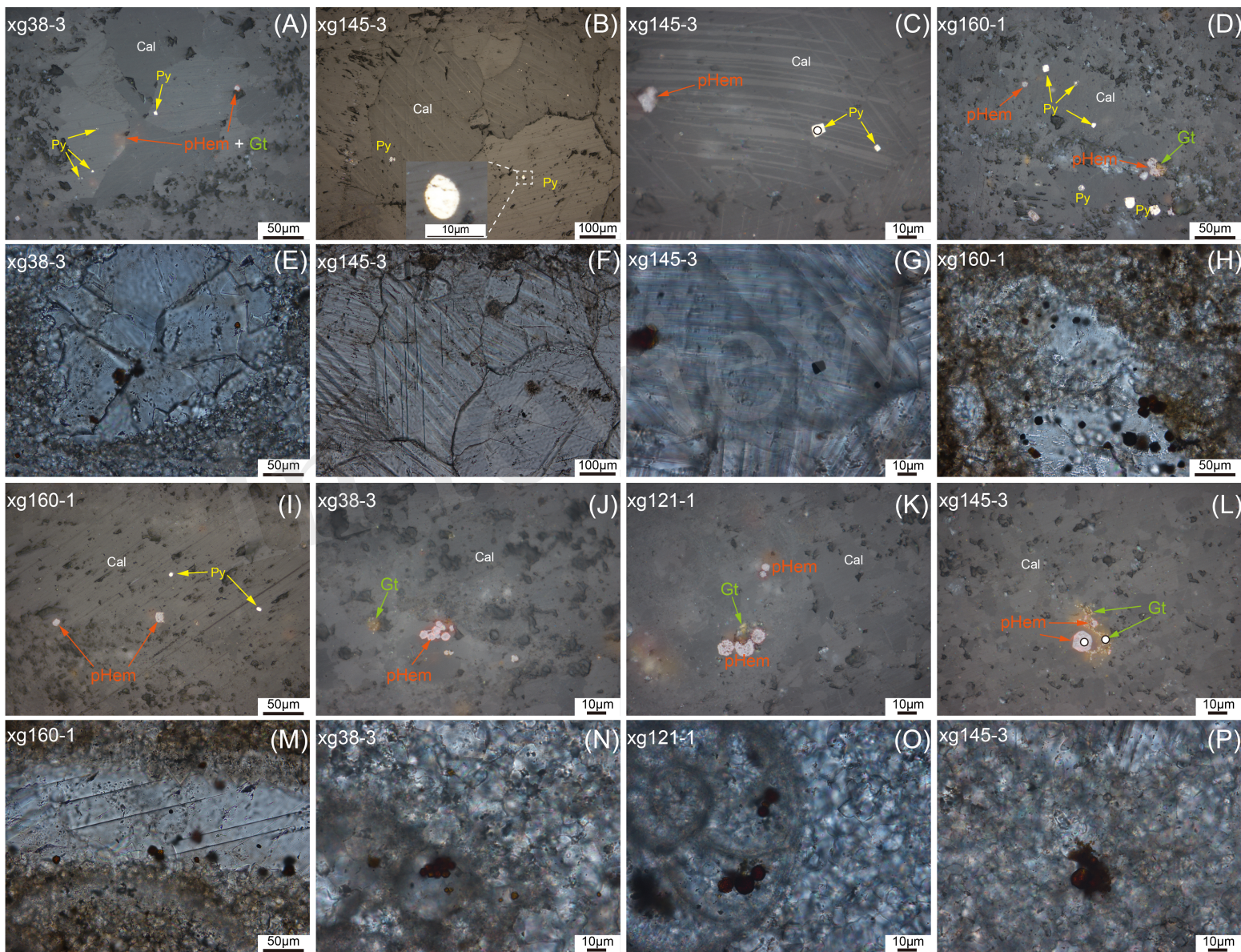


Figure 3.JPEG

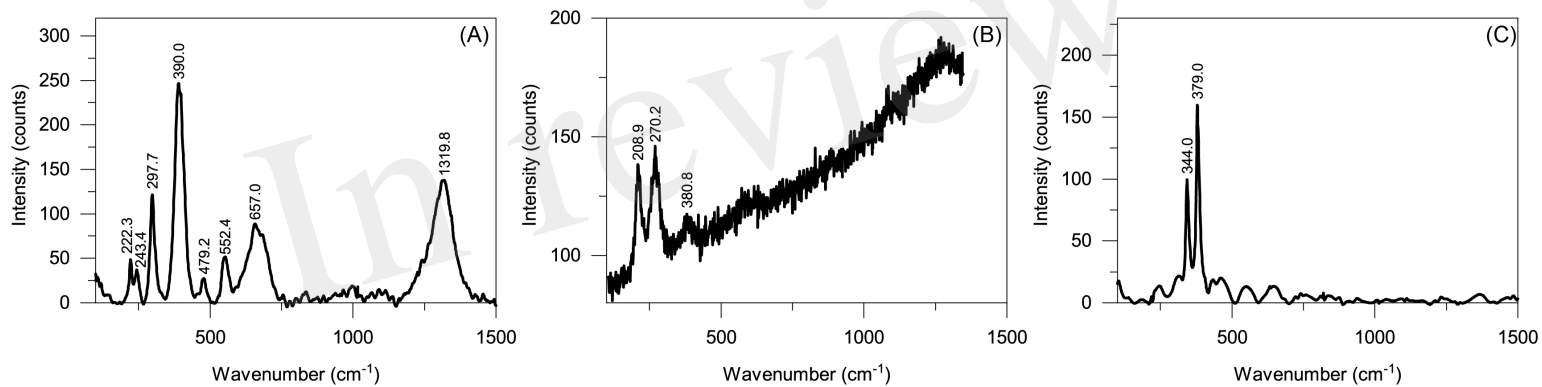


Figure 4.JPEG

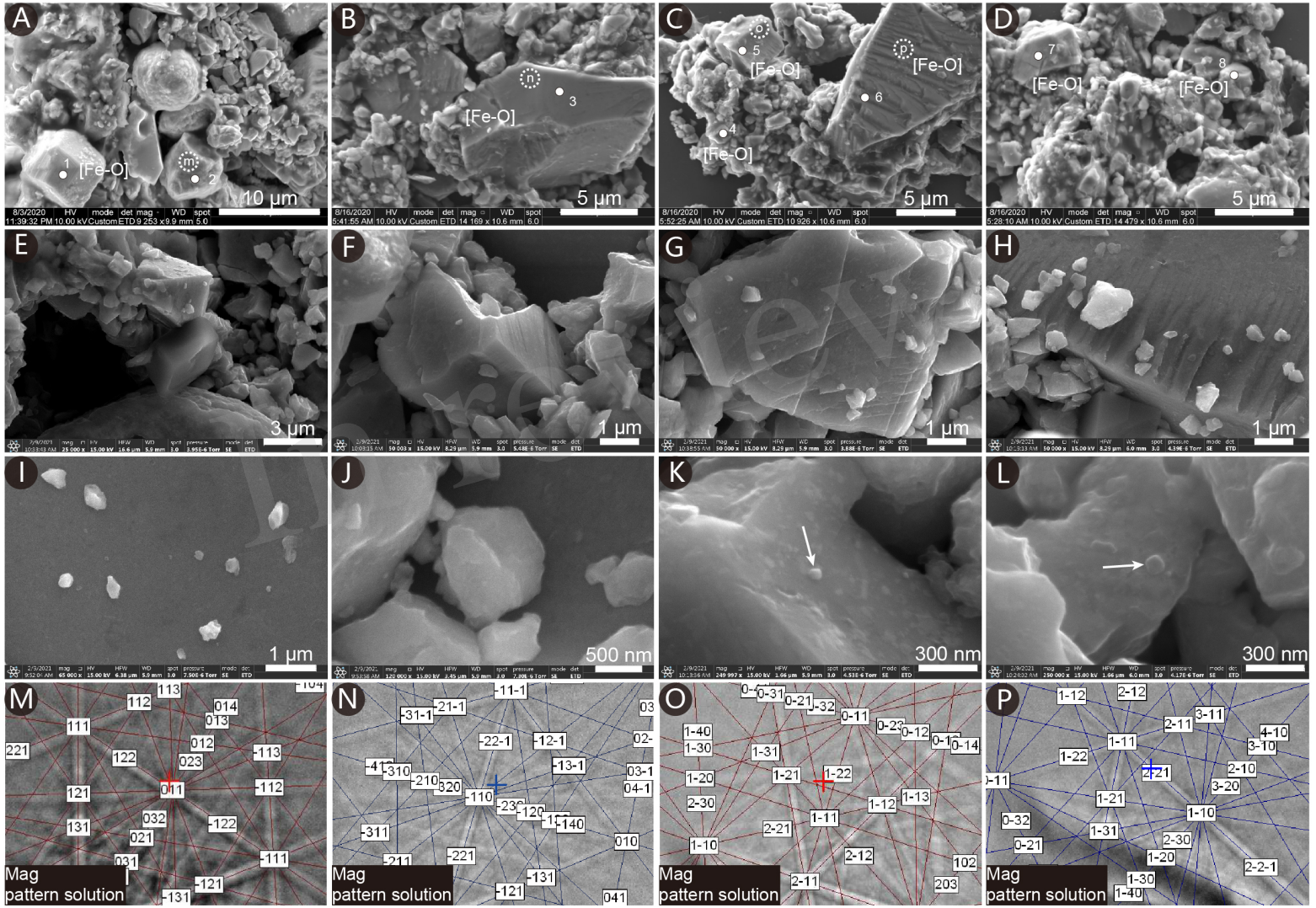


Figure 5.JPEG

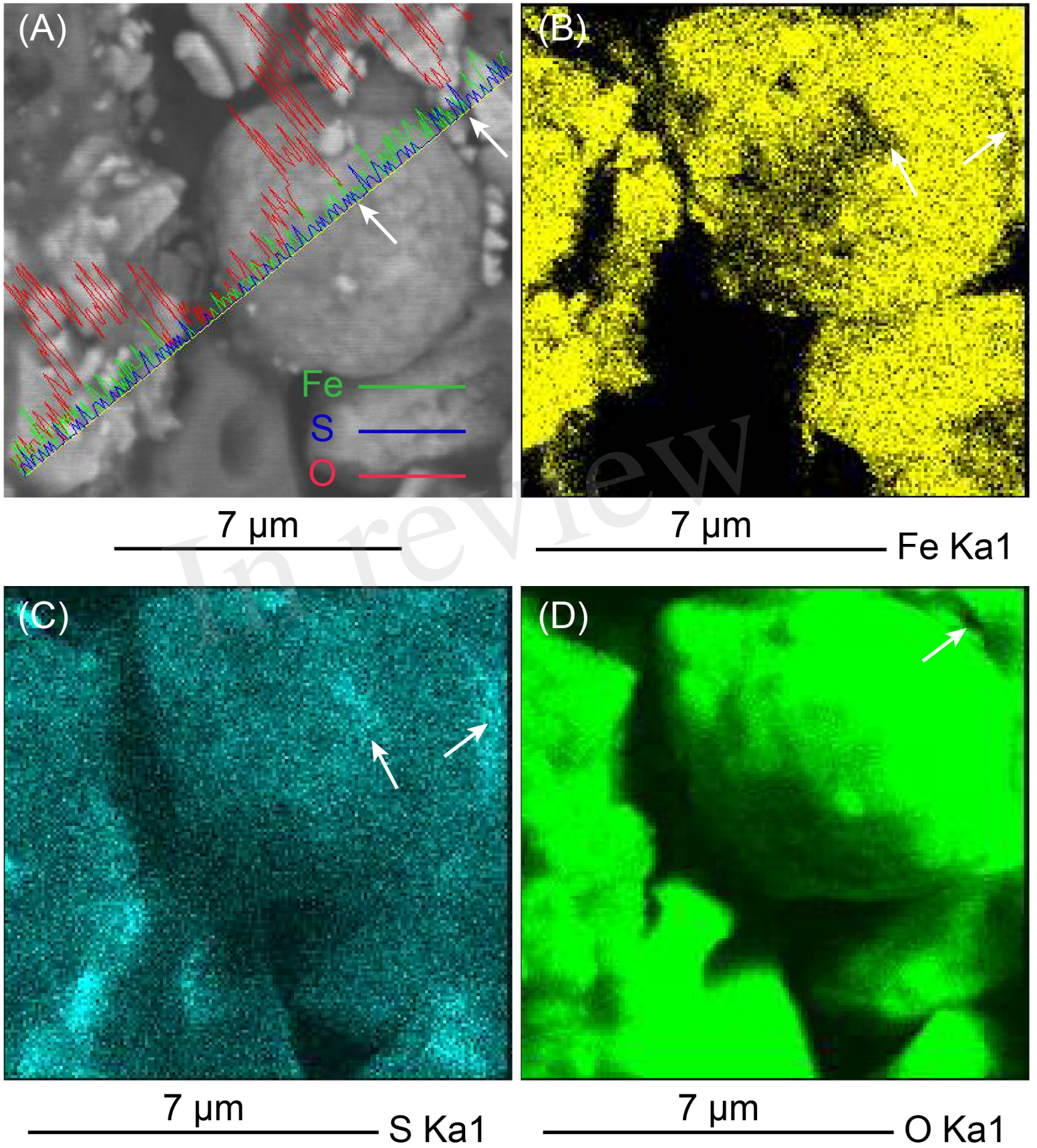


Figure 6.JPEG

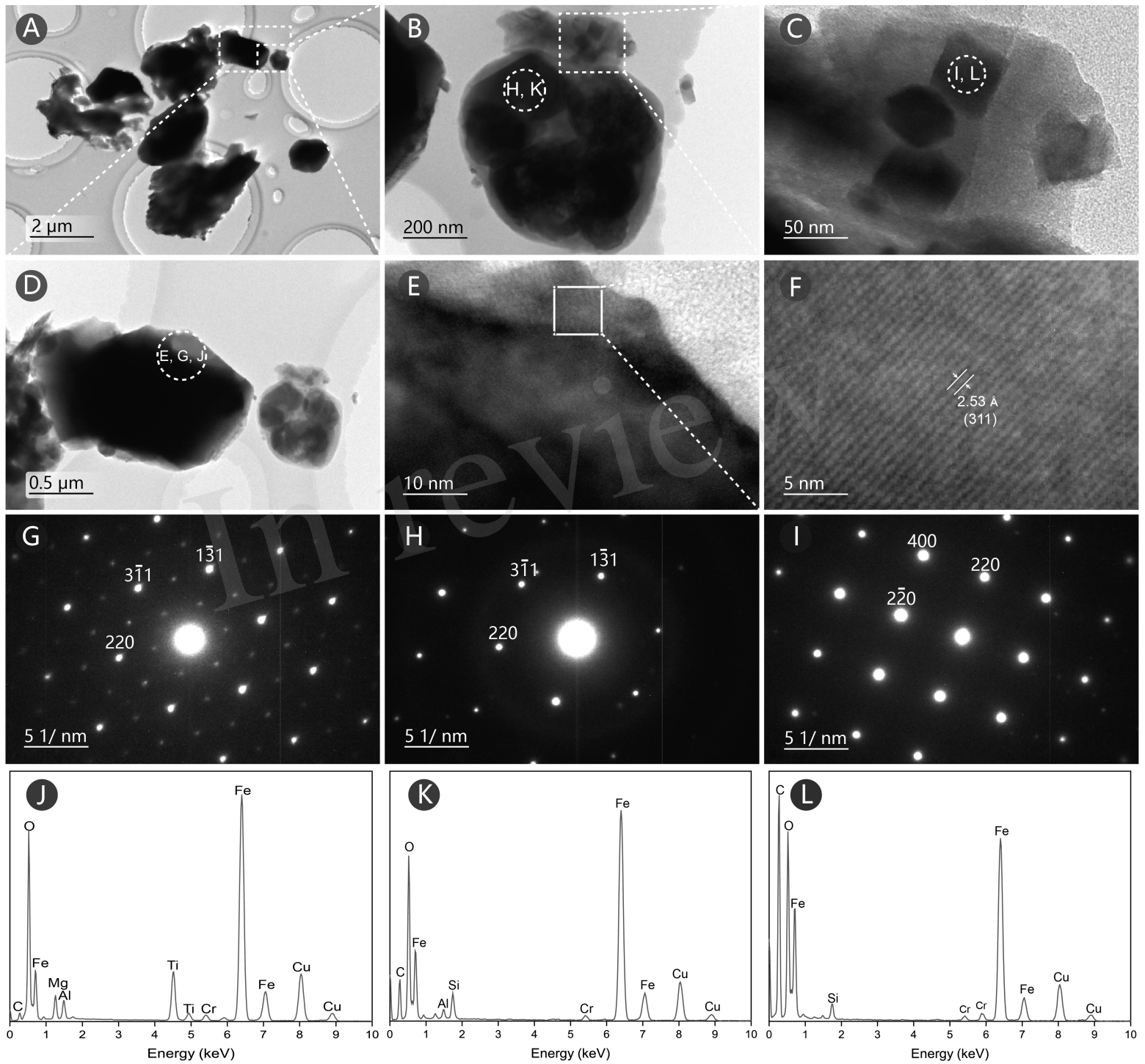
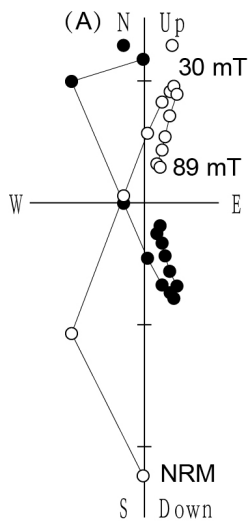
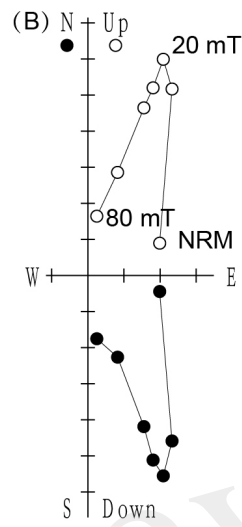


Figure 7.JPEG



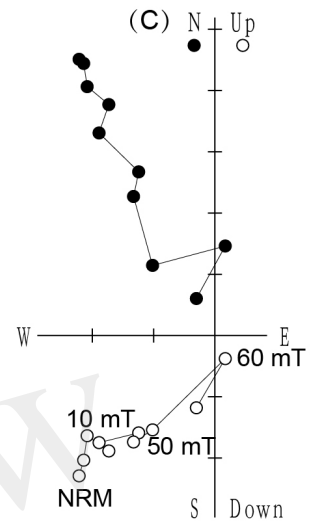
xg0-3-IS

Scale:  $1e-4$  A/m



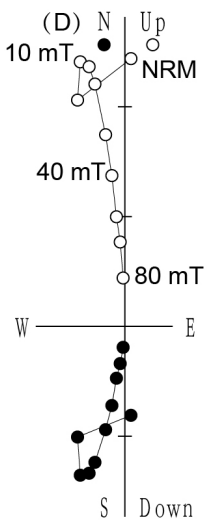
xg38-3-IS

Scale:  $1e-5$  A/m



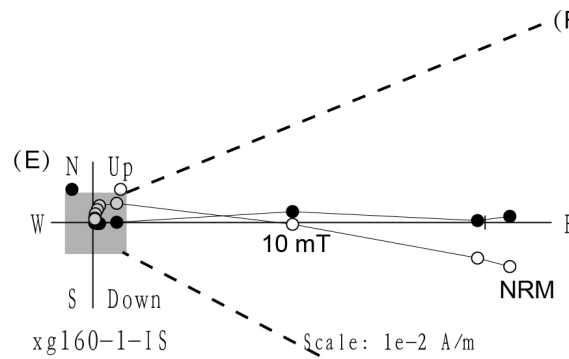
xg121-2-IS

Scale:  $1e-5$  A/m



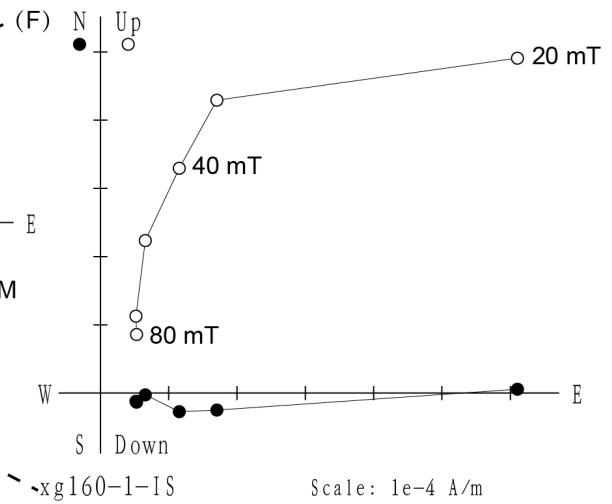
xg145-2-IS

Scale:  $1e-4$  A/m



xg160-1-IS

Scale:  $1e-2$  A/m



xg160-1-IS

Scale:  $1e-4$  A/m

## Supplementary Material

### 1 Supplementary Figures

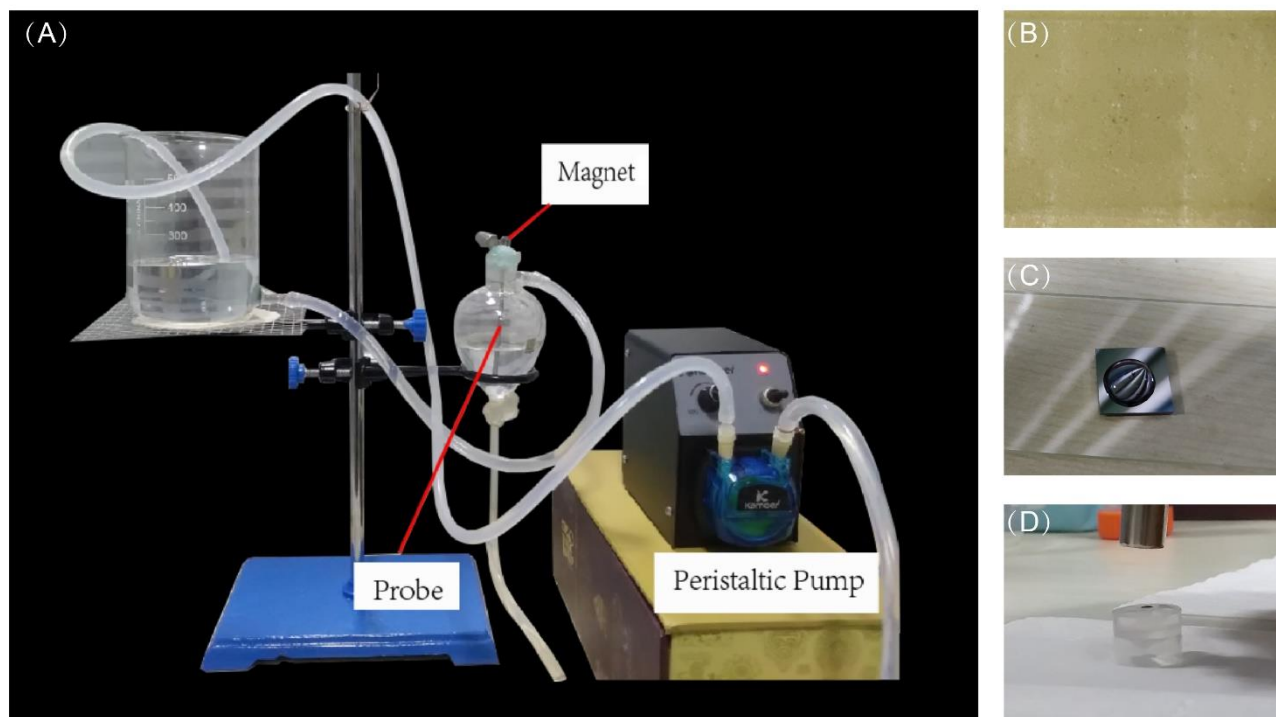


**Figure S1.** (a) Magnetic extraction apparatus. (b) Samples preparation of thin sections using resin as an adhesive; Magnetic extracts dropping on a monocrystalline silicon wafer (c), and TEM grid (d).

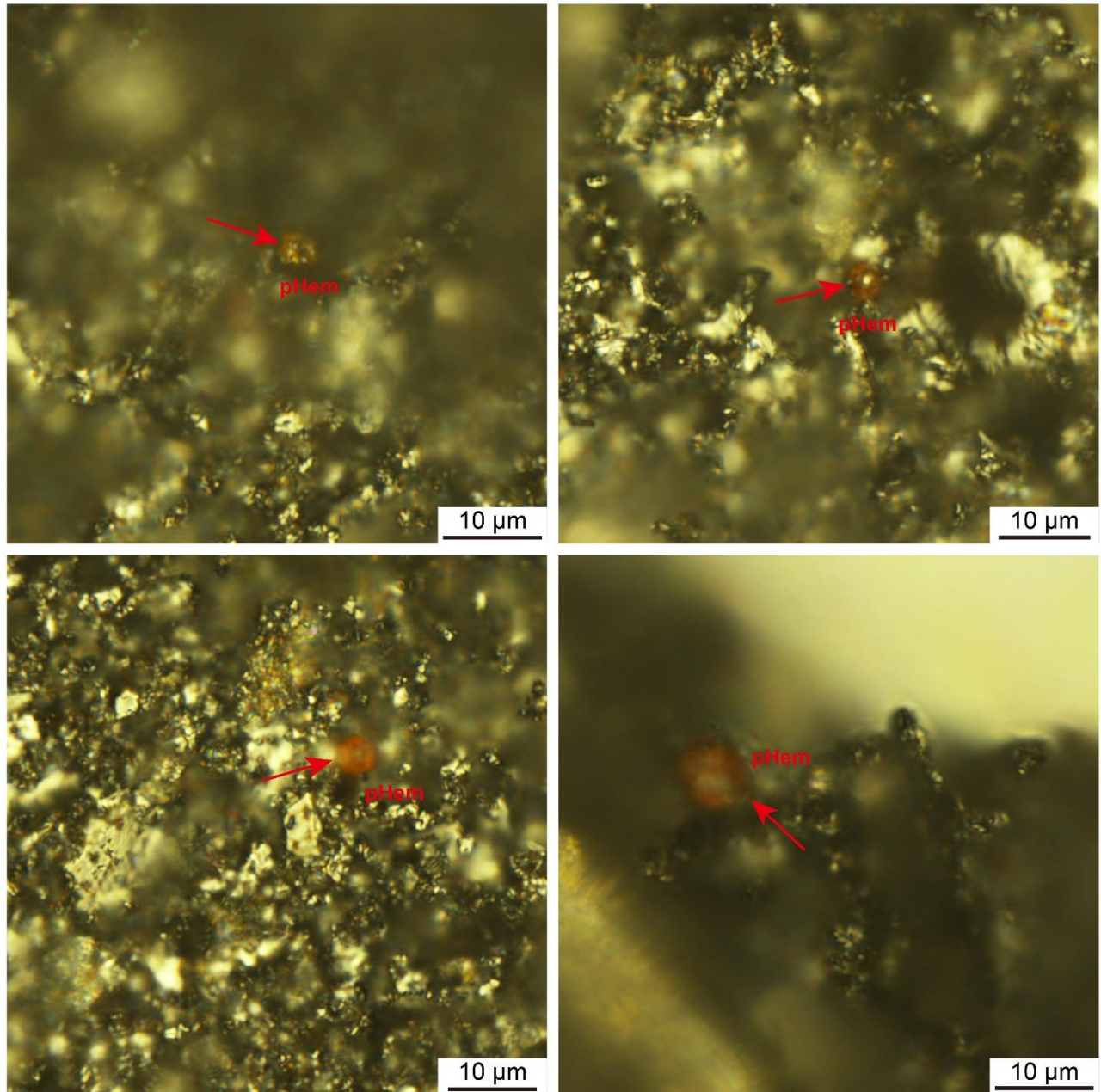


**Figure S2.** Photomicrographs illustrating the iron oxide spherules of magnetic extracts from the Zongpu carbonate rocks in the Gamba area under reflected light. pHem = pigment hematite.



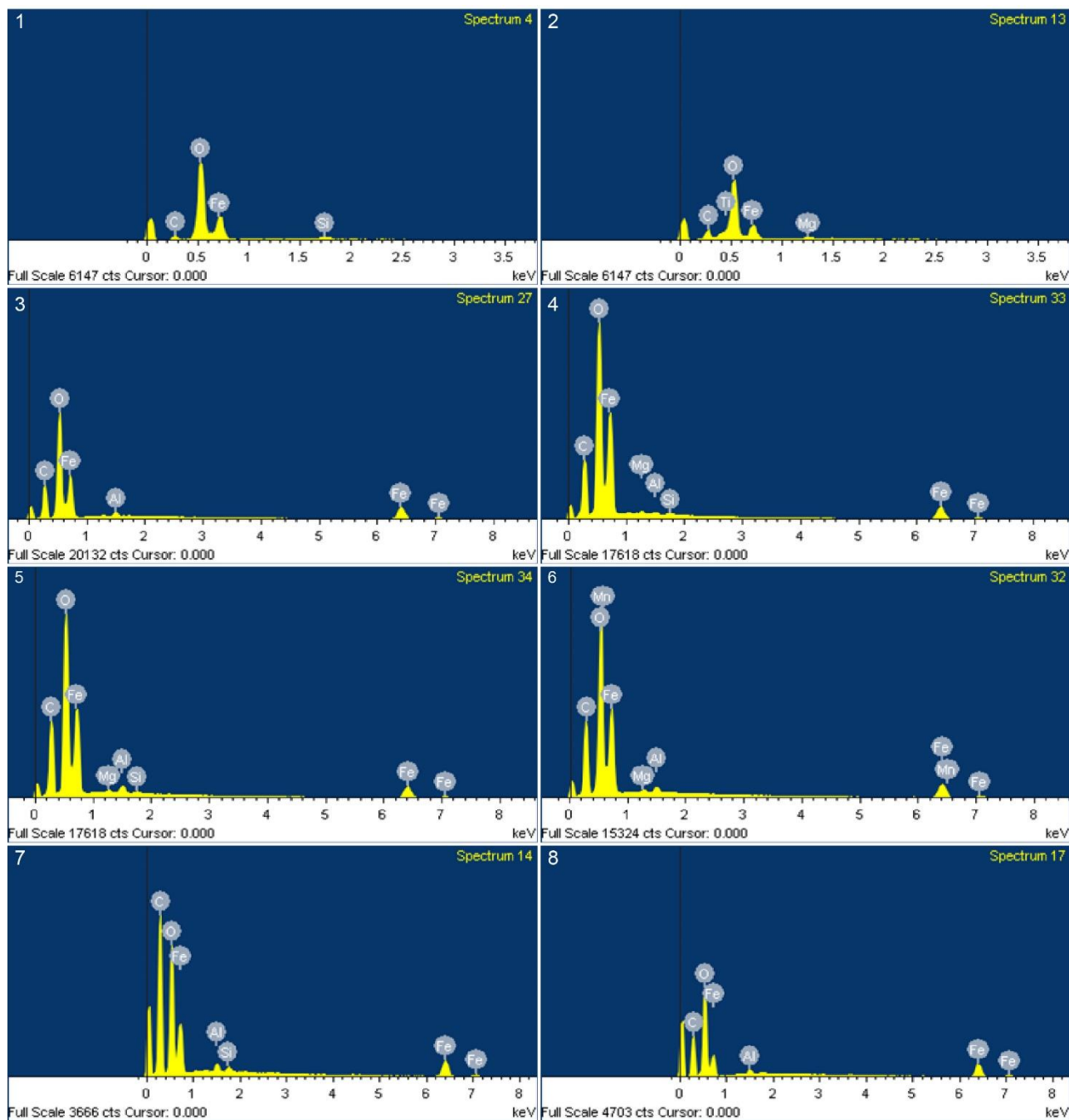


**Figure S3.** EDS analysis results of the spots shown in Figure 4.

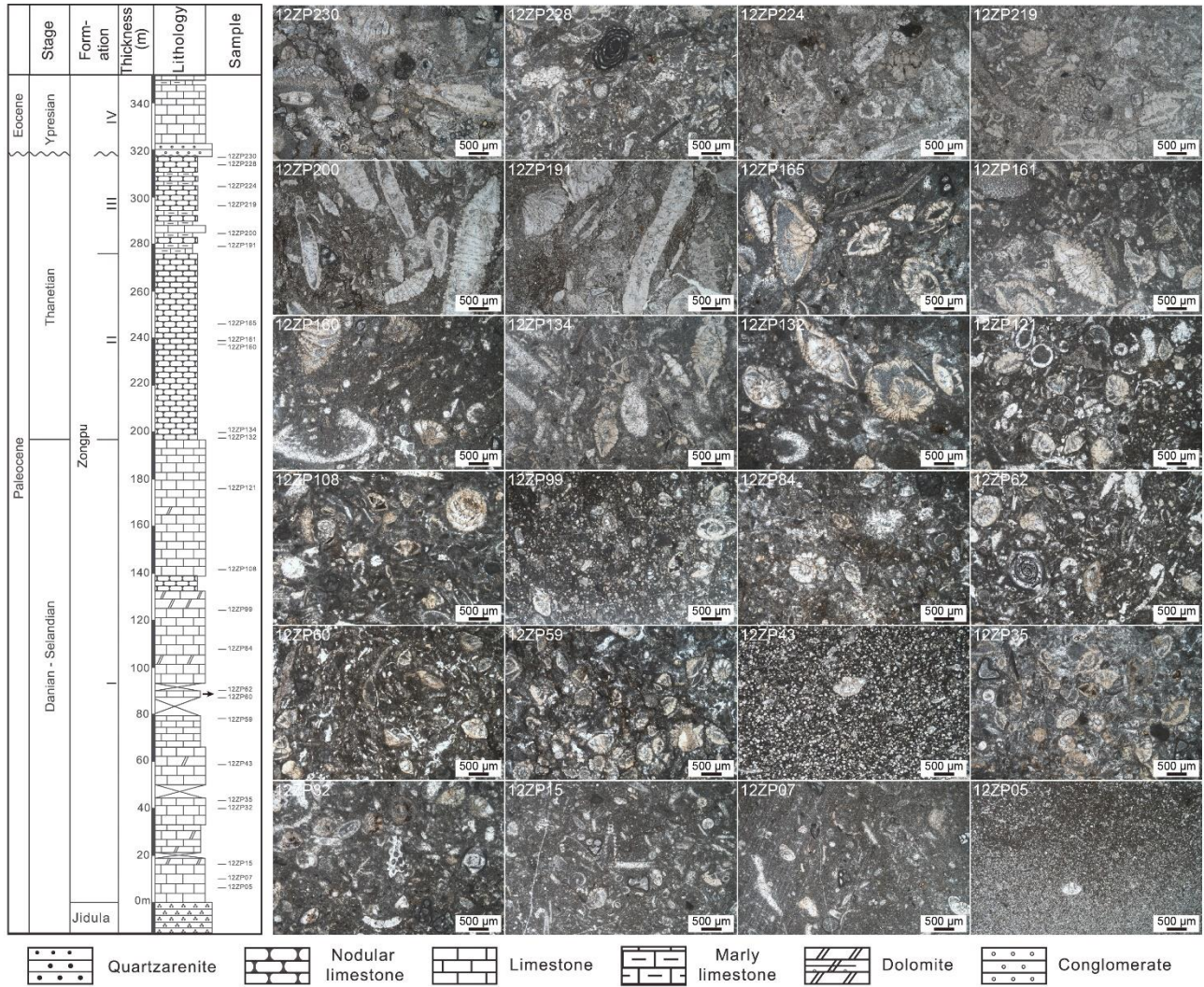


**Figure S4.** Left: Lithostratigraphy of the Zongpu Formation. Partial sampling localities of rock magnetic measurements in Huang et al. (2017a) were indicated, modified after Li et al. (2015) and Huang et al. (2017a). Right: Corresponding photomicrographs, collected from Li and Hu (2020). Please see [www.csdata.org](http://www.csdata.org) for more micrographs and detailed descriptions.

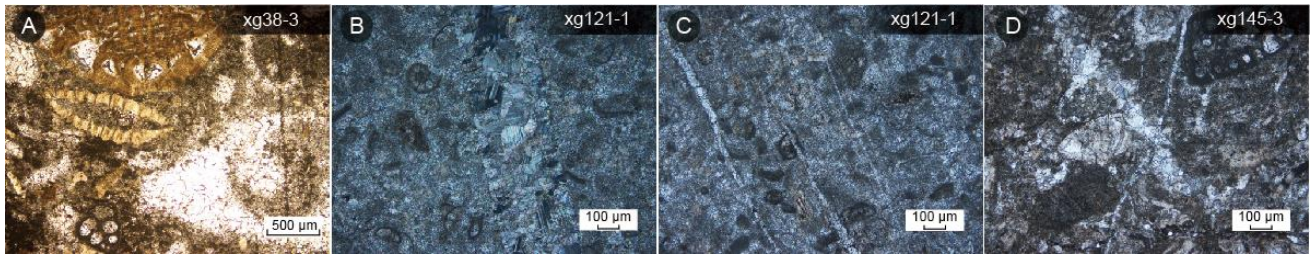


**Figure S5.** The larger benthic foraminifera from section A of Yi et al. (2011) in plane-polarized light (a) and reflected light (b-d). The localities of sampling collection are marked in Figure 1C.

## 2 Reference

- Huang, W., Lippert, P.C., Jackson, M.J., Dekkers, M.J., Zhang, Y., Li, J., et al. (2017a). Remagnetization of the Paleogene Tibetan Himalayan carbonate rocks in the Gamba area: Implications for reconstructing the lower plate in the India-Asia collision. *Journal of Geophysical Research-Solid Earth* 122(2), 808-825. doi: 10.1002/2016jb013662.
- Li, J., Hu, X., Garzanti, E., An, W., and Wang, J. (2015). Paleogene carbonate microfacies and sandstone provenance (Gamba area, South Tibet): Stratigraphic response to initial India-Asia continental collision. *Journal of Asian Earth Sciences* 104, 39-54. doi: 10.1016/j.jseaes.2014.10.027.
- Li, J., and Hu, X. (2020). A photomicrograph dataset of Late Cretaceous to Early Paleogene carbonate rocks in Tibetan Himalaya. *China Scientific Data* 5. doi: 10.11922/csdata.2020.0072.zh.